DETECTION OF PHOTONS IN THE HERA-B RICH

P. Križan
J. Stefan Institute and University of Ljubljana, Slovenia
for the HERA-B RICH Group*

ABSTRACT

The tests carried out with the photon detector of the ring imaging Cherenkov detector for the HERA-B experiment are reviewed. Results of on-the-bench tests of the employed photomultiplier tubes are reported together with early commissioning measurements with the HERA proton beam.

1 Introduction

The HERA-B experiment [1] aims at measuring: CP violation in $B^0 \to J/\psi K^0_S$ and $B^0 \to \pi^+\pi^-$ decays, $B^0_s \bar{B}^0_s$ mixing and $B\bar{B}$ decays with two leptons in the final state. The B mesons will be produced in collisions of 920 GeV/c protons with a fixed target. The target consists of eight wires in the halo of the proton beam in order not to disturb experiments measuring ep collisions.

One of the essential components of the spectrometer is the ring imaging counter (RICH), with the prime function of separating kaons from pions [1–4]. In what follows, we shall briefly describe the essential components of the RICH counter, and will then discuss in detail the detection of photons.

2 The HERA-B RICH

The main purpose of the ring imaging Čerenkov counter in the HERA-B experiment is the tagging of the B meson flavor. Tagging of the B^0, or the $\overline{B^0}$ meson, is accomplished by identifying the charged

*The HERA-B RICH Group is a collaboration of the University of Texas at Austin, University of Barcelona, LIP Coimbra, Northwestern University, Evanston, DESY Hamburg, University of Houston, J. Stefan Institute, Ljubljana, and University of Ljubljana.

kaon into which the associated B meson decayed. The momentum distribution of charged kaons, resulting from decays of the B mesons, is shown in Fig. 1. Identifying the charged kaon essentially

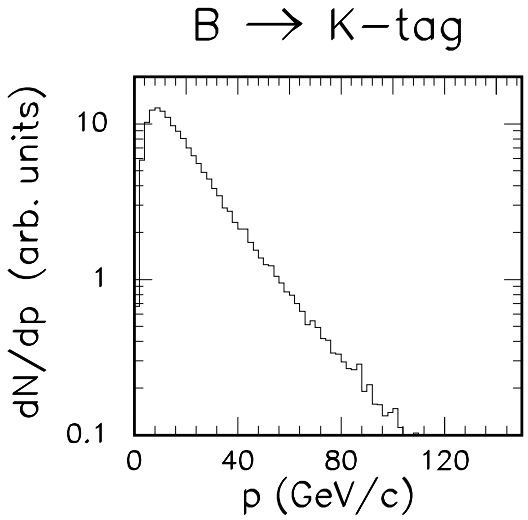

Figure 1: The momentum distribution of charged kaons produced in decays of B mesons associated to the production of a B^0 or $\overline{B^0}$ meson by proton nucleus interactions at HERA-B.

means separating it from the pion of the same momentum. Since the momentum is accurately measured in other components of the HERA-B detector, the separation in mass is equivalent to the separation in velocity, for which the RICH counter is employed.

Perfluorobutane gas (C_4F_{10}) has been chosen for the HERA-B RICH radiator, since it combines a relatively high-refractive index and a low dispersion. In this gas, the Čerenkov radiation threshold momenta for pions and kaons are at 2.7 GeV/c and 9.6 GeV/c, respectively. For $\beta = 1$ particles, the Čerenkov angle is 51.5 mrad, while the $\pi - \mathrm{K}$ difference in Čerenkov angle is 6 mrad at 20 GeV/c and falls to 0.9 mrad at 50 GeV/c.

The set-up of the counter is schematically shown in Fig. 2. The two spherical mirror halves are tilted, i.e., the center of curvature of each half mirror is displaced relative to the target position, by which photons are reflected to photon detectors well outside the charged particle flux.

The 108 m^3 vessel for the C_4F_{10} gas radiator has been constructed from stainless steel, except for the particle entry and exit windows (1 mm Al), and the photon exit windows (UVT perspex). Also, two-beam shrouds close the gas volume around the two beam pipes for protons and electrons are constructed. The purification and circulation system for the C_4F_{10} gas has been constructed at CERN and was commissioned at DESY. It is worth noting that the initial filling of the volume amounts to about 1100 kg of C_4F_{10}.

Two mirror systems, a spherical and a planar one, are made of hexagonal and rectangular units, respectively. The hexagonal mirror segments with 11.4 m radius of curvature have been produced

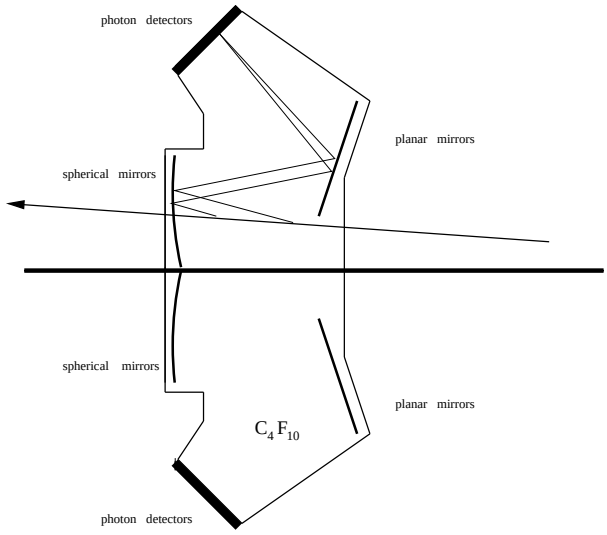

Figure 2: *The HERA-B RICH.*

of 7 mm thick grinded glass. The mirror quality has been determined upon delivery by measuring the radius of curvature for each segment, and the fraction of reflected light, as well as by recording a Ronchi image to check the homogeneity of the mirror surface. The reflectivity was required to exceed 85% in the wavelength interval of 250 - 600 nm. Each spherical mirror segment is supported at three points, two of which can be moved, and are motor driven via a transmission mechanism with a feed through to the exterior of the vessel. The planar mirrors are made of float glass, thus being significantly cheaper at the required optical quality. By making use of the data gathered on all the mirror segments, it was possible to group them in the tiling scheme according to their optical quality and resolution requirements [5].

3 Photon Detector

Initially, two wire chamber based photon detectors were considered, a CsI photocathode in a MWPC and a TMAE-based detector with 10 cm deep, and 8 x 8 mm^2 unit cells. After the considerable success of on-the-bench and beam tests [6–8], the detectors were tested in a high-rate environment as expected in the HERA-B experiment. Both wire chamber-based detectors had to be abandoned; the TMAE detector showed a prohibitive decrease of avalanche gain due to aging effects [9,10], while the CsI photocathode could not be routinely produced and maintained with sufficiently high quantum efficiency, in addition to problems with rates in excess of a few kHz per pixel [11,12].

The final photon detector considered was the Hamamatsu multianode R5900 M16 and M4 photomultiplier tubes, which became available just at the time when it was realised that an alternative solution is needed. The M16 version has 16 pads of 4.5 x 4.5 mm^2 each, with a 12-stage, metal-foil

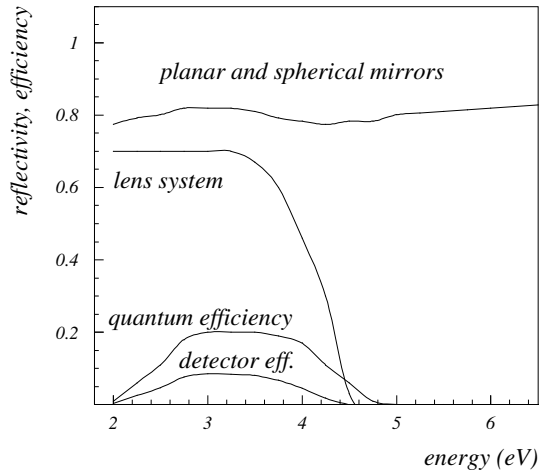

Figure 3: *Reflectivity of planar and spherical mirrors and the detection efficiency of the photon detector as a function of photon energy. The photon detector efficiency is a product of the photomultiplier tube quantum efficiency, the photoelectron detection efficiency and the transparency of the optical system.*

dynode system [13]. The M4 version has four pads of 9 x 9 mm^2 each and ten dynodes. The quantum efficiency of the photocathode with a borosilicate window has a broad plateau in the wavelength region between 300 nm and 500 nm with a maximum value of 20% (Fig. 3). The UV-extended version has a UV transparent window, which shifts the low wavelength cut-off to about 250 nm. The other PMT characteristics such as the required cathode high voltage ($\leq$ 1000 V), the current amplification (10^7), dark current ($\sim$ 1 nA), pulse rise time (0.8 ns), transit time spread (0.3 ns) [13], are also satisfactory.

The outer dimensions of the PMT are 28 x 28 mm^2, so the photocathode occupies only about 30% of the surface. Due to the smaller photocathode surface compared to the photomultiplier cross section, a two lens demagnification system (2:1) was designed (Fig. 4) [14]. The lenses are made of UVT perspex with high transparency over most of the wavelength region, where the photocathode is sensitive (Fig. 3). The angular acceptance of the optical system is also satisfactory and is uniform for incident angles below about 110 mrad [15]. In addition to increasing the active area, the lens system also adjusts the required pixel size in the central detector region (9 x 9 mm^2) to the PMT pad size 4.5 x 4.5 mm^2. The outer detector region with lower occupancy and looser resolution requirements, uses the M4 version of the tube with two times larger pads (9 x 9 mm^2) with the same lens system, such that the pixel size amounts to 18 x 18 mm^2.

The base board accepts four PMT's and provides positioning. In addition it houses the voltage divider, signal lines, and the front-end electronics consisting of 16-channel boards based on the

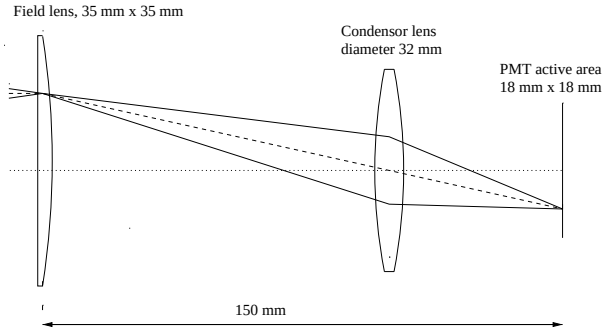

Figure 4: *The optical system for light collection and demagnification. The two rays shown in full line correspond to photons with incident angles of* ± 100 *mrad.*

ASD8 chip [16]. In Fig. 5, a photograph of a fully equipped basic module for the M16 photomultiplier tubes is presented.

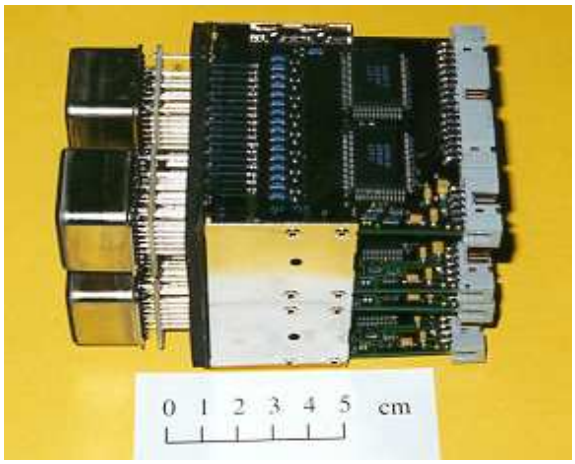

Figure 5: *Fully equipped photomultiplier basic module with the Hamamatsu R5900 photomultiplier tubes type M16.*

In order to reduce the contribution of spherical aberration to the overall resolution of the Čerenkov angle, an optimal surface of the Čerenkov photon detector has been calculated [17,18]. Each half-detector (upper and lower) consists of five flat supermodules placed in order to approximate the optimal surface, which is close to the shape of a flattened (ellipsoidal) cylinder. Such an arrangement also ensures better acceptance for the Čerenkov photons, which should be incident onto the flat supermodules at angles below 110 mrad.

From the data available on the quantum efficiency, mirror reflectivities, window and optical system transmissions (see Fig. 3), one calculates the merit factor $N_0 = 43$ cm^{-1}, such that the expected number of photons for particles approaching the velocity of light amounts to $N_{det} = N_0 L \sin^2\vartheta = 31$ with $L = 2.7$ m and $\vartheta = 51.5$ mrad. The expected single photon resolution is 0.7 mrad and 1 mrad for the regions occupied by M16 and M4 PMT's, respectively.

4 Measurements and Results

4.1 Multianode PMT as a Single Photon Counter

In the initial set of measurements [20] the single photon counting properties of the tube were investigated, in particular the efficiency for single photon detection as well as the background count rate. In this phase three multianode PMT's were tested; one with borosilicate glass window (serial no. 6A19C4) and two with UV transparent windows (serial no. 5M26C6 and serial no. 6C22C5). The tubes were of the 16-channel photomultiplier tube assembly type which includes a voltage divider circuit (Hamamatsu type H6568).

In the experimental set-up shown in Fig. 6 it was established that the tube allows for good single photoelectron detection as may be seen in Fig. 7. The average pulse height on each of the pads

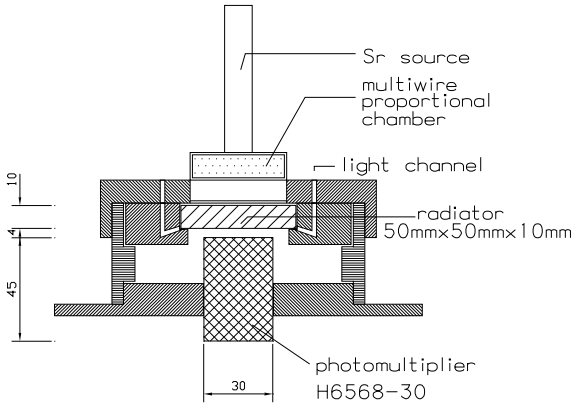

Figure 6: *The set-up for testing the PMT properties on the bench. Čerenkov photons, emitted by* ^{90}Sr *β particles in a solid radiator, are used as a stable light source [21].*

is shown in Fig. 8. These data were obtained by allowing a small leak of daylight into the crystal radiator from which the photon reached the photocathode more or less uniformly illuminating its surface.

The bleeder chain was optimized by varying the composition of the 13 resistors [22]. Very little dependence of rate at the high voltage plateau was seen when varying the fraction of the 1 MΩ to 560 kΩ resistors. Somewhat better results were obtained with the first three steps of 1 MΩ resistors, followed by ten 560 kΩ resistors. This bleeder chain was then adopted for the M16 photomultiplier tube. For the M4 photomultiplier a similar voltage divider was chosen, where again the first three resistors had twice the value of the other eight.

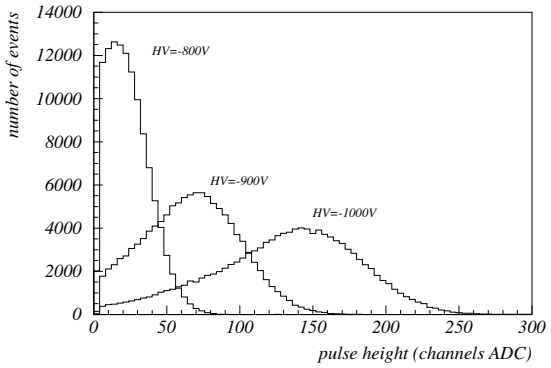

Figure 7: *The measured pulse height distributions of the M16 PMT due to single photoelectrons for different high voltage values.*

Cross talk has been estimated by observing simultaneous pulses on adjacent pads, when the pulse on one pad has been recorded to be above a certain threshold. The pulse height spectra, triggered by pad number 7 are shown in Fig. 9. The cross talk is estimated from this figure to be 0.2% between direct neighbors and only 0.1% between diagonal neighbors.

Ageing was studied [20] by illuminating the photocathode pads with a 5 W neon bulb through a small hole at one side of a 1 m long, 10 cm diameter black plastic tube with the PM on the other side. No reduction of the 3 MHz counting rate has been observed over a 30-day period of continuous illumination and operation.

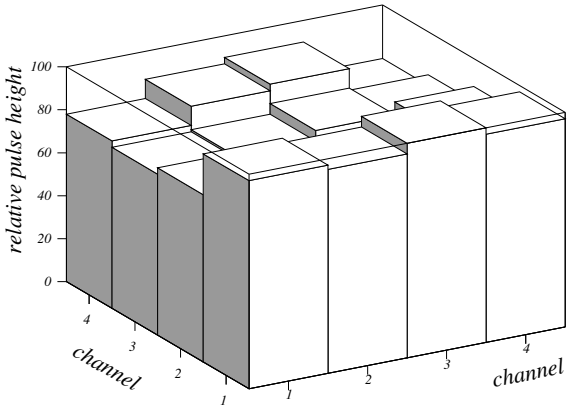

Figure 8: *Lego plot of the average single photoelectron pulse heights normalised to the pad with the largest average pulse height.*

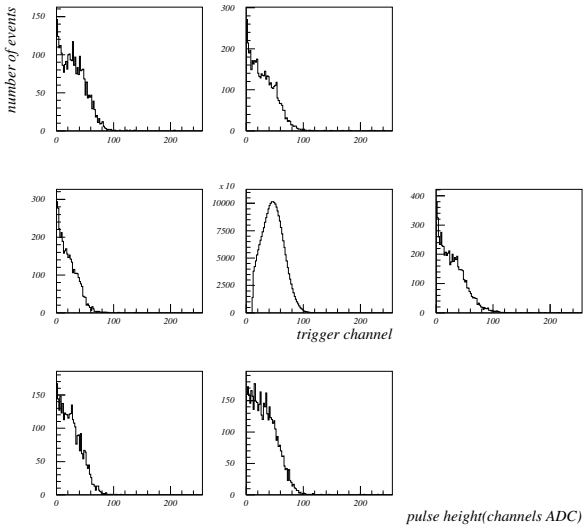

Figure 9: *Cross talk has been measured by triggering with one of the channels and observing simultaneous pulses on six neighbouring channels.*

4.2 Results of Quality Assessment Tests

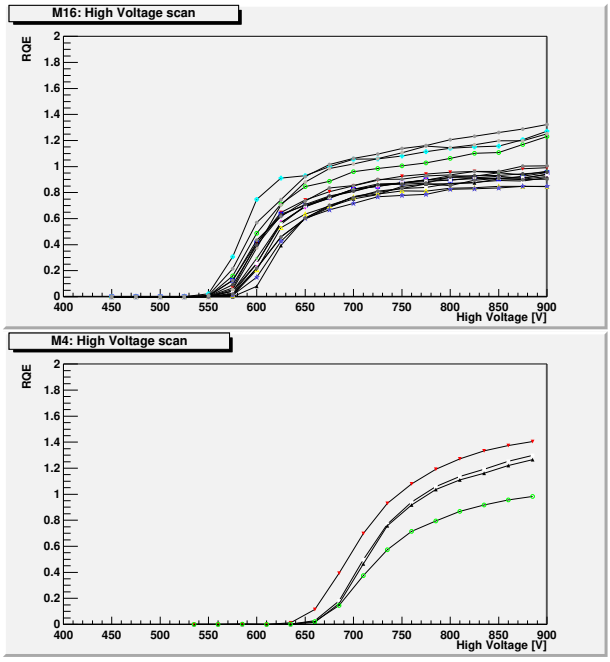

Figure 10: *Dependence of the suitably normalized rate (channel count rate divided by 1000 and 4000 for M16 and M4 PMT's, respectively) as a function of the high voltage for all channels of a representative M16 (above) and M4 (below) photomultiplier tube.*

Tests of all the 2305 PMT's (1543 M16's and 762 M4's) have been made in the laboratory prior to the installation in the photon detector [23]. The apparatus employed is similar to the one shown in Fig. 6. Again, Čerenkov photons produced by β electrons of the ^{90}Sr source were used as a stable light source. In this case four tubes were tested at the same time, of which one was used as a reference. For each photomultiplier tube, the source and background rates were recorded as a function of high voltage and threshold setting (Figs. 10-12). On the basis of these tests, the photomultipliers have been grouped according to similar high voltage characteristics, allowing all PMT's within a group to be connected to the same high voltage, thus maximising the efficiency for the given, much smaller number of independent HV channels [19]. The results obtained for the optimal high voltage, as well as for the relative PMT sensitivity, were compared to values provided by the manufacturer, and a good agreement was found [23].

Figure 13 gives the distribution of M4 and M16 photomultipliers versus their recommended high voltage value as obtained in the quality assessment tests. This value is seen to be larger for M4's than for M16's, which is a consequence of the smaller number of dynodes (10 for M4's compared to 12 for M16's). The distributions of photomultipliers depending on their normalized count rate (channel count rate divided by 1000 and 4000 for M16 and M4 PMT's, respectively) at

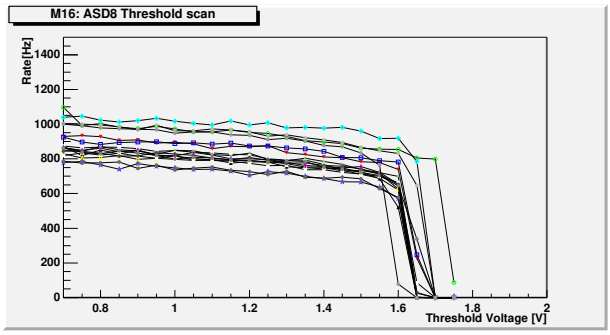

Figure 11: *Dependence of the count rate on the threshold voltage for a typical M16 photomultiplier tube.*

the recommended value of high voltage are shown in Fig.14 separately for M16's and for M4's.

Finally Fig.15 shows the time dependence of the rate per channel of the reference M4 and M16 photomultipliers in the quality assessment tests. The count rate decrease is consistent with the known decay rate of the ^{90}Sr source.

From the quality assessment tests relative surface sensitivity of each tube could be determined, after correcting for a slightly nonuniform illumination of the surface. An example for each of the PMT types is shown in Fig. 16.

To further investigate the variation of sensitivity over the photomultiplier surface, a scan was carried out for selected PMT's by using a light beam spot of about 20 μm diameter [24]. From Fig. 17 the pad and dynode channel structure can clearly be seen.

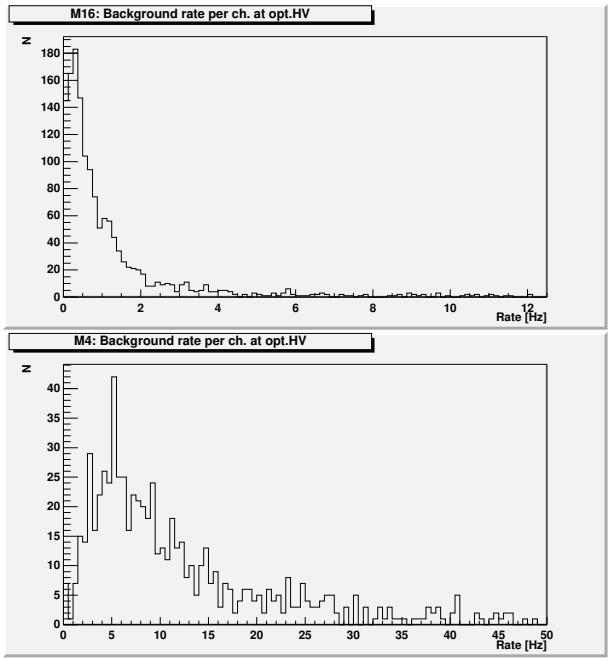

Figure 12: *Distribution of M16 (top) and M4 (bottom) channels depending on their background count rate.*

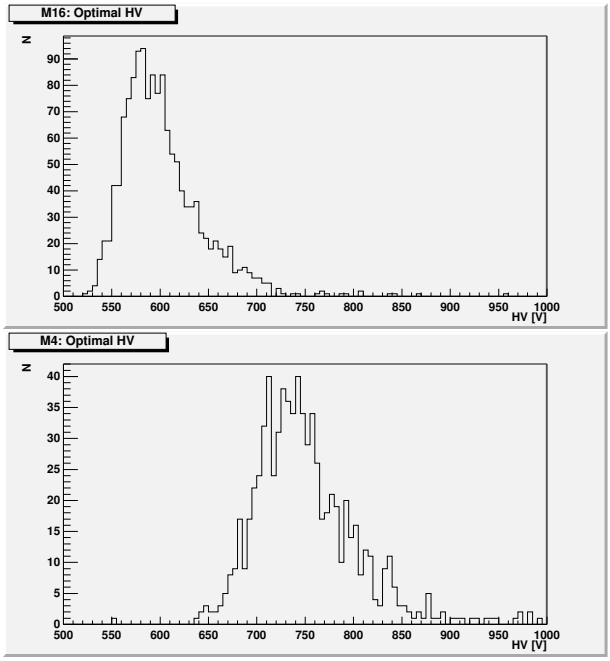

Figure 13: *Distribution of M16 (top) and M4 (bottom) photomultipliers depending on the value of their recommended high voltage.*

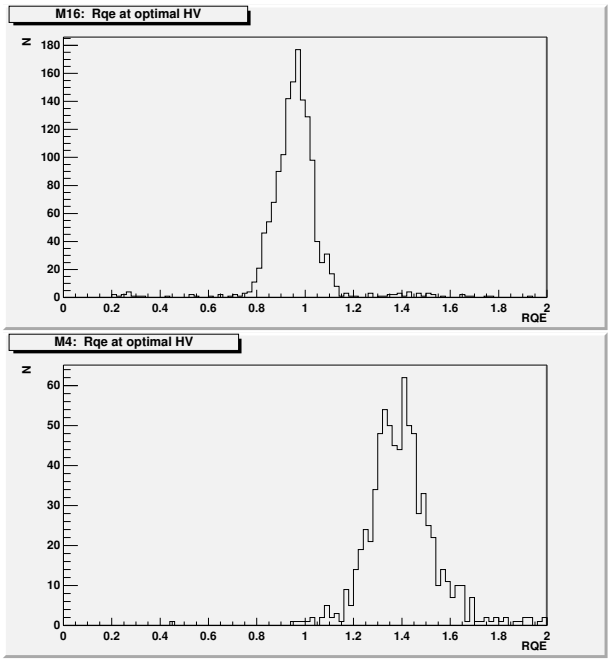

Figure 14: *Distribution of M16 (top) and M4 (bottom) photomultipliers according to their normalized count rate (RQE) at the recommended voltage.*

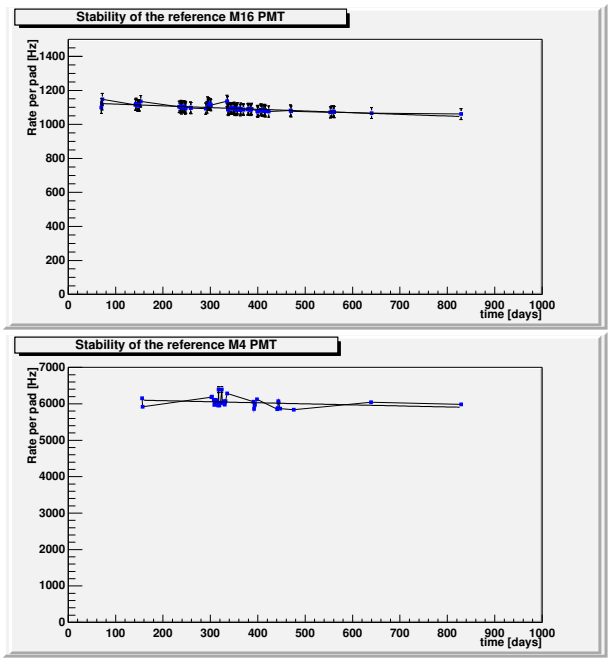

Figure 15: *The time dependence of the count rates of the reference photomultipliers; M16 (top diagram), M4 (below). The curves represent the radioactive decay of* ^{90}Sr.

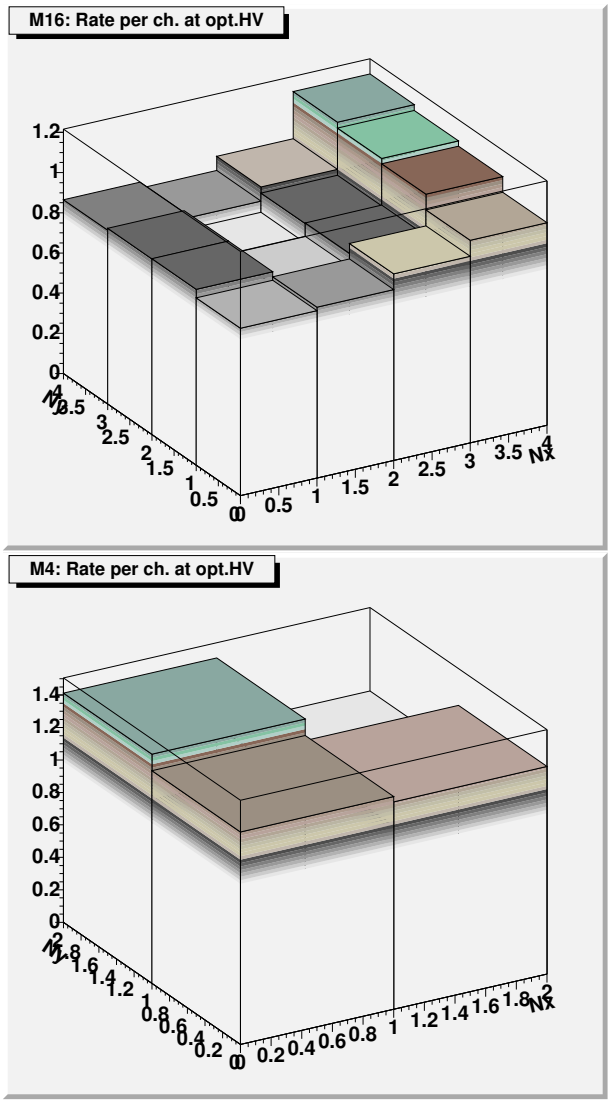

Figure 16: *Relative sensitivity of each pad of representative M16 and M4 photomultipliers as determined by illuminating the whole surface.*

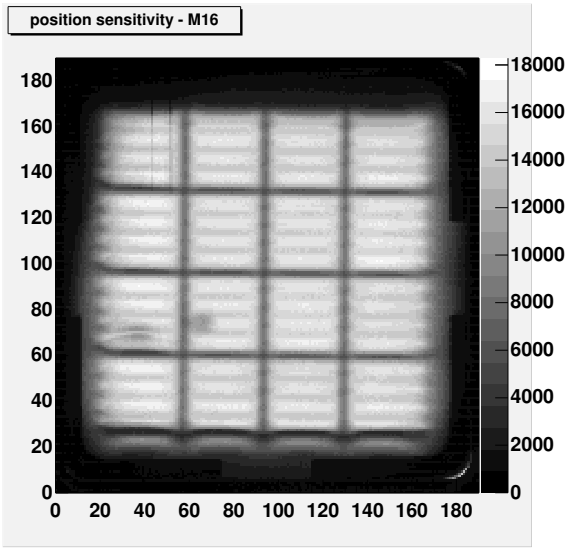

Figure 17: *Sensitivity of a M16 PMT surface when scanned by a light beam spot of about 20 μm diameter.*

4.3 Test Measurements In Situ

With the photon detectors in their proper position in the HERA-B spectrometer, the photomultipliers cabled to the readout system and with freon as Čerenkov radiator, the commissioning of the system became possible. Fig. 18 gives the count rate versus high voltage for one of the M16 and one of the M4 photomultipliers. It is seen that the curves measured in situ with the HERA proton beam agree nicely with the ^{90}Sr source measurements. The occupancy is shown in Figure 19, where the region occupied by M16 PMT's is clearly distinguished from the region occupied by M4 PMT's. We also note that only about 0.3% of the nearly 30,000 channels were found to be noisy, and were excluded from further analysis.

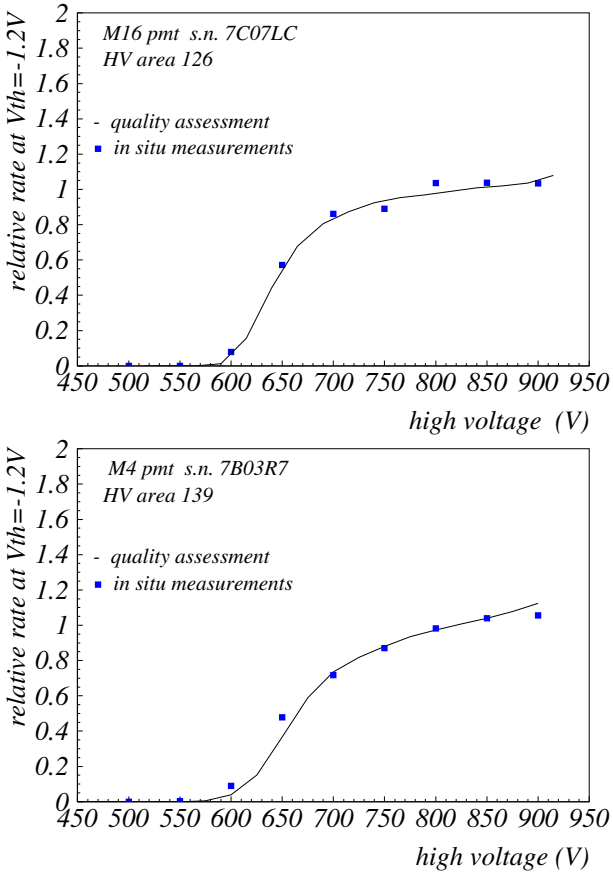

Figure 18: *The plateau curves for a M16 (top) and a M4 (bottom) photomultiplier tube. The data labelled 'in situ' represent values measured during the photon detector testing in its final position, while the curves labelled "quality assessment" correspond to measurements made in the laboratory during on-the-bench quality tests. The data are normalised to the average of the three points at 750 V, 800 V, and 850 V.*

The performance of the RICH detector was also checked by varying the interaction rate of the wire target. In a set of measurements, the response of the detector was recorded at target rates

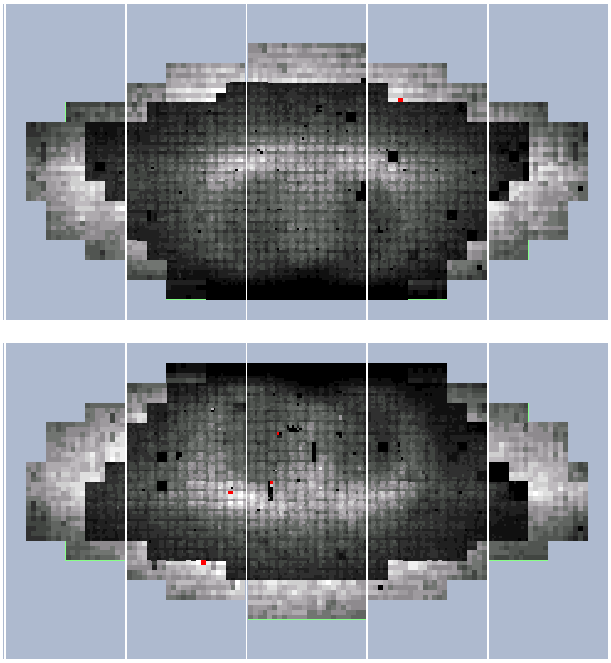

Figure 19: *The occupancy of the upper and lower photon detectors shows the region occupied by M16 (inner region) and M4 PMT's (outer region).*

from 1 MHz up to the design value of 40 MHz. In Fig. 20, the accumulated number of hits on the photon detector as a function of target interaction rate is presented, and a good linearity can be seen.

Due to the nonavailability of the information from the particle tracking system, the Čerenkov ring radii were deduced by finding the rings which best fit the detected hits on the photon detector. Only events which depict well-separated Čerenkov rings were employed in a simple analysis [25]. In the analysis, one counts the detected photons per Čerenkov ring by looking at appropriate events (two of which are shown in Figs. 21 and 22) and measures the corresponding ring radius. The number of counted hits per Čerenkov ring is plotted as a function of the measured Čerenkov angle in Fig. 23. The lines drawn on the plot correspond to a hypothesis that $31 \pm \sqrt{31}$ photons are radiated from particles approaching the velocity of light.

For each of the rings recorded in Fig. 23, we calculated the photon detector response parameter N_0. The resulting distribution is shown in Fig. 24. We observe that the average value of the photon detector response parameter, as well as the average number of detected photons per ring, are consistent with expectations.

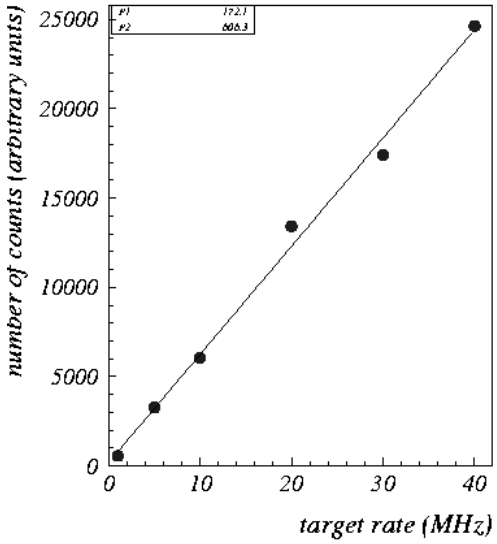

Figure 20: *Accumulated number of hits on the photon detector versus target interaction rate. Noisy channels (in total about 0.3%) are suppressed.*

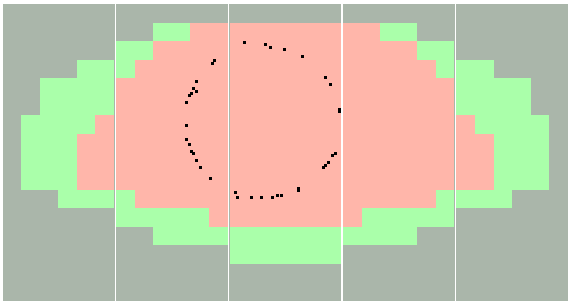

Figure 21: *Display of an event on the lower photon detector with a single Čerenkov ring consisting of 33 detected photons. From the ring radius Čerenkov angle of* 51.9 ± 0.5 mrad *is deduced for which* 31 ± 2 *detected photons would be expected.*

5 Summary

A detector of Čerenkov photons for a high-rate environment of the HERA-B experiment was designed, tested, installed, and commissioned. A preliminary data analysis shows that the design goals, a figure of merit N_0=43 cm^{-1}, resulting in 31 detected photons on a saturated Čerenkov ring, was met. We also note that the resolution as determined from a stand-alone ring search analysis [26] is consistent with the design values of 0.7 mrad and 1 mrad for M16 and M4 tubes, respectively.

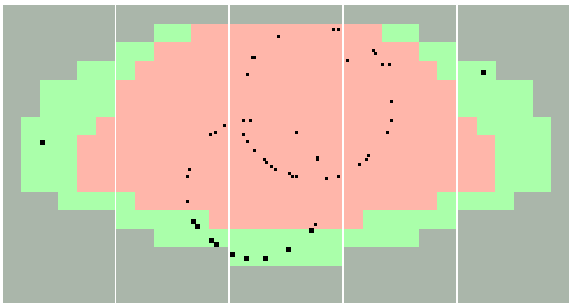

Figure 22: *Two intersecting Čerenkov rings, one with 22 photons detected by four and sixteen channel photomultiplier tubes, a measured Čerenkov angle of* 45.5 ± 0.5 mrad *and expected number of* 23.8 ± 1.5 *hits, and a ring with 27 photons detected exclusively by sixteen channel photomultiplier tubes,* 49.8 ± 0.5 mrad *Čerenkov angle and expected* 28.5 ± 1.8 *hits.*

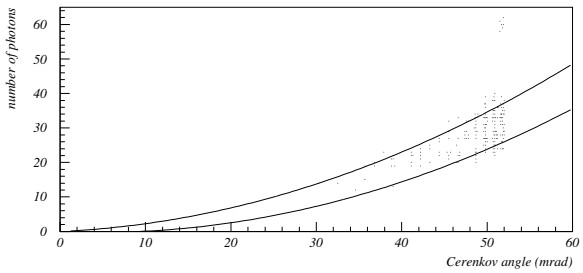

Figure 23: *Measured (data points) and expected (*$\pm\sigma$ *curves) number of detected photons versus Čerenkov angle for nearly 200 rings which could be well-separated. Some events are also seen with two times more detected photons per ring than expected. They are due to Čerenkov radiation of an overlapping* e^+e^- *pair.*

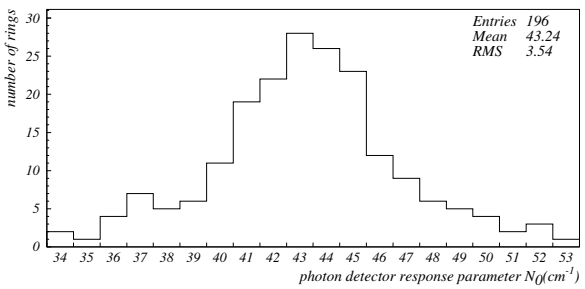

Figure 24: *The distribution of the photon detector response parameter* N_0.

References

[1] T. Lohse et al. Proposal for HERA-B, DESY PRC-94/02, May 1994.

[2] P. Križan, R. Mankel, D. Ressing, S. Shuvalov, M. Spahn, Nucl. Instr. Meth. in Phys. Res. A351 (1994) 111-131.

[3] J.L. Rosen, Nucl. Instr. Meth. in Phys. Res. A408(1998)191.

[4] S. Korpar et al., Nucl. Instr. and Meth. in Phys. Res. **A433** (1999) 128-135.

[5] D. Dujmić, K. Reeves, HERA-B RICH Note 97-182, Hamburg 1997
HERA-B Note.

[6] T. Hamacher et al., Nucl. Instr. and Meth. in Phys. Res. **A371** (1996) 289-294.

[7] P. Križan, M. Cindro, V. Cindro, S. Korpar, G. Omahen, A. Stanovnik, M. Starič, Nucl. Instr. and Meth. in Phys. Res. **A364** (1995) 243-252.

[8] P. Križan, S. Korpar, M. Starič, A. Stanovnik, M. Cindro, D. Škrk, M. Zavrtanik, T. Hamacher and E. Michel, 1994 IEEE NSS Conference Record, Volume 2 (1995) 985-988.

[9] J. Pyrlik at al., Nucl. Instr. and Meth. in Phys. Res. **A414** (1998) 170-181.

[10] S. Korpar, P. Križan, A. Stanovnik, M. Starič, D. Škrk, IEEE Transactions on Nuclear Science, Vol. 46, Number 3 (1999) 317-320.

[11] P. Križan, S. Korpar, M. Starič, A. Stanovnik, M. Cindro, D. Škrk, M. Zavrtanik, T. Hamacher, E. Michel, Nucl. Instr. and Meth. in Phys. Res. **371** (1996) 151-154.

[12] P. Križan et al., Nucl. Instr. and Meth. in Phys. Res. **A387** (1997) 146-149.

[13] Hamamatsu Data Sheets for R5900-M16 and R5900-M4 Photomultipliers.

[14] J. McGill, R. Schwitters, HERA-B Note 96-278, DESY, Hamburg (1996); D. Broemmelsiek, Nucl. Instr. and Meth. in Phys. Res. **A433** (1999) 136-142.

[15] R. Eckmann, M. Ispirian, S. Karabekyan, J. McGill, R. Schwitters, HERA-B Note 97-162, DESY, Hamburg (1997).

[16] F.M. Newcomer et al., IEEE Transactions on Nuclear Science, **40**,4 (August 1993)630.

[17] P. Križan, M. Starič, Nucl. Instr. and Meth. in Phys. Res. **A379** (1996) 124-129.

[18] R. Schwitters, HERA-B Note 97-088, DESY, Hamburg (1997); D. Dujmić, R. Schwitters, HERA-B Note 98-052, DESY, Hamburg (1998).

[19] J. Pyrlik and K. Lau, HERA-B Note 97-182, DESY, Hamburg (1997).

[20] P. Križan, S. Korpar, R. Pestotnik, M. Starič, A. Stanovnik, E. Michel, C. Oehser, W. Schmidt-Parzefall, A. Schwarz, T. Hamacher, D. Broemmelsiek, J. Pyrlik, Nucl. Instr. and Meth. in Phys. Res. **A394** (1997) 27-34.

[21] V. Cindro, S. Korpar, P. Križan, A. Stanovnik, M. Starič, D. Škrk, Nucl. Instr. and Meth. in Phys. Res. **A337** (1994) 609-612.

[22] S. Korpar, R. Pestotnik, P. Križan, IJS Report, IJS-DP-7615, Ljubljana (1997); HERA-B Note 97-079, DESY, Hamburg (1997).

[23] S. Korpar et al., Proc. of the 2nd Conference on Photodetection, Beaune, France, June 1999, to be published in Nucl. Instr. and Meth. in Phys. Res.

[24] S. Korpar et al., IJS Report, IJS-DP, Ljubljana (1999).

[25] D. Škrk, Doctoral thesis, Univerza v Ljubljani, Fakulteta za matematiko in fiziko, Oddelek za fiziko, Ljubljana, June 1999.

[26] R. Schwitters, HERA-B Note 99-215, DESY, Hamburg (1999).